



Development of antibacterial nanocomposites by combination of bacterial cellulose/chitin nanofibrils and all-natural bioactive nanoparticles

Yuqi Mei^a, Yunyi Yang^a, Ruohang Gao^a, Mengyue Xu^{a,b}, Qing Li^a, Zhili Wan^{a,c,*},
Xiaoquan Yang^a

^a Laboratory of Food Proteins and Colloids, School of Food Science and Engineering, Guangdong Province Key Laboratory for Green Processing of Natural Products and Product Safety, South China University of Technology, Guangzhou, 510640, China

^b Laboratory of Physics and Physical Chemistry of Foods, Wageningen University, Bornse Weiland 9, 6708WG, Wageningen, the Netherlands

^c Overseas Expertise Introduction Center for Discipline Innovation of Food Nutrition and Human Health (111 Center), Guangzhou, 510640, China

ARTICLE INFO

Handling Editor: Dr. Xing Chen

Keywords:

Bacterial cellulose nanofibrils
Chitin nanofibrils
Glycyrrhizic acid
Nanocomposites
Natural active small molecules
Nanoparticles

ABSTRACT

In this study, a functional composite membrane was facilely fabricated by using a dual nanofibril system of bacterial cellulose (BC) and chitin (CH) nanofibrils as bio-based building blocks. The BC-CH membranes with enhanced antibacterial activity were constructed by incorporation of all-natural bioactive nanoparticles (GBTPs), which were formed by spontaneous molecular interactions of three naturally occurring active small molecules, i. e., glycyrrhizic acid (GA), berberine (BR), and tannic acid (TA). The microstructure, physicochemical properties, and antibacterial behaviors of the resulting BC-CH-GBTPs nanocomposites were then characterized. The obtained results showed that the GBTPs with a diameter of around 50–100 nm and membrane matrix were bound by non-covalent interactions, and the addition of GBTPs did not compromise the structural integrity and thermal stability of the composites, which retained good mechanical properties. Furthermore, the addition of GBTPs led to a rougher surface structure and increased the water contact angle of the membrane surfaces from 48.13° to 59.80°. The antimicrobial tests indicate that the BC-CH-GBTPs nanocomposites exhibited significant inhibitory effects against *Escherichia coli* and *Staphylococcus aureus*, showing a satisfactory antibacterial ability. These results suggest that the BC-CH-GBTPs nanocomposites based on all-natural, plant-based building blocks, hold promising potentials as active packaging materials for sustainable applications.

1. Introduction

With increasing global environmental concerns, the development of a new generation of nanocomposite materials and processes based on the principle of sustainability, eco-efficiency, and green chemistry, have received extensive attention in many industrial fields (Barhoum et al., 2019; Min et al., 2022). Many natural, renewable, and biodegradable polymer nanomaterials, such as cellulose nanofibrils, are being explored to create high-performance nanocomposites or nanopapers with strong mechanical performance and environmentally friendly attribute (Klemm et al., 2011; Wan et al., 2016; Kontturi et al., 2018; Chen et al., 2020; Fan et al., 2020). Among them, bacterial cellulose (BC) is a natural nanoscale three-dimensional network cellulose synthesized by microorganisms, mainly *Acetobacter xylinum* species (Lu et al., 2020), which possesses edibility, high purity, excellent mechanical strength,

biocompatibility, and biodegradability, rendering it a versatile nanomaterial for applications in various fields including food, paper, and biomedicine (Shi et al., 2014; Swingler et al., 2021). Nevertheless, the highly hydrophilic nature of BC due to the abundance of surface hydroxyl groups and the lack of functional properties (e.g., antibacterial activity) largely limit its potential use as an amenable membrane material for food and biomedical applications. To overcome these limitations, the widely adopted approach is to create the BC-based nanocomposites with various functional polymers or nanoscale building blocks, such as protein nanoparticles (Li et al., 2020), metal nanoparticles (Zhang et al., 2010), carbon nanotubes (Kang et al., 2012), and polyaniline nanoparticles (Fei et al., 2019), which can confer a range of functional features such as antibacterial, photocatalytic, and conducting abilities to the resultant BC nanocomposites (Wan et al., 2016; Wahid et al., 2021).

* Corresponding author. Laboratory of Food Proteins and Colloids, School of Food Science and Engineering, Guangdong 6 Province Key Laboratory for Green Processing of Natural Products and Product Safety, South China 7 University of Technology, Guangzhou, 510640, China.

E-mail address: zhiliwan@scut.edu.cn (Z. Wan).

<https://doi.org/10.1016/j.crfs.2023.100584>

Received 21 June 2023; Received in revised form 30 August 2023; Accepted 31 August 2023

Available online 1 September 2023

2665-9271/© 2023 Published by Elsevier B.V. This is an open access article under the CC BY-NC-ND license (<http://creativecommons.org/licenses/by-nc-nd/4.0/>).

Chitin (CH) is the second most abundant biopolymer widely distributed in nature, especially in the exoskeletons of shellfish and insects and the cell walls of fungi (e.g., mushrooms). The molecular chains of CH are arranged in an orderly manner with high strength and high modulus through strong intermolecular hydrogen bonding (Butchosa et al., 2013). In addition, as a natural polymer from biological sources, CH has good biocompatibility and biodegradability, and is a green and environment-friendly raw material (Ding et al., 2014). However, the layered structure of chitin molecules readily lead to the formation of crystal lattices with strong intermolecular hydrogen bonding, which makes them insoluble in water and thus largely limits the applicability of CH (Ahmad et al., 2020). To address this issue, the colloidal suspensions of CH nanocrystals in water have been prepared by strong acid hydrolysis or TEMPO-mediated oxidation of semicrystalline chitin (Fan et al., 2008; Bai et al., 2022), which can be used for reinforcing polymer nanocomposites. Zhou et al. prepared the BC-based nanocomposites by incorporating three different types of CH nanocrystals, and found that only the partially deacetylated CH nanocrystals can endow the nanocomposites with significant antibacterial activity (Butchosa et al., 2013). Compared to CH nanocrystals, the homogeneous CH nanofibrils can be more easily produced in large amounts only by simple mechanical treatments under acid conditions (pH 3–4) (Fan et al., 2008; Ifuku and Saimoto, 2012), which therefore are considered to a more efficient and sustainable reinforcement nanomaterial for nanocomposite applications. Recently, Yang et al. prepared composite films by combination of BC and CH nanofibers, and demonstrated that the CH nanofibers can improve the mechanical strength and barrier property of the BC-CH composite films (Yang et al., 2020). Although the partially deacetylated CH nanofibrils are reported to have antibacterial activity (Xu et al., 2019), these original CH nanofibrils without any chemical modifications do not show obvious antibacterial effect due to the low amount of the cationic amino groups. Therefore, to develop multifunctional BC-CH nanocomposite materials such as antibacterial membranes, it is necessary to further introduce functional building blocks such as antibacterial nanoparticles into the composites to enhance their antibacterial properties for practical applications. In comparison with the synthetic antibiotics or metallic nanoparticles with potential negative effects on environment and human health (Kraemer et al., 2019), the natural antibacterial nanomaterials, especially these obtained from the naturally occurring bioactive molecules that have high biological activities, are more highly desired to be used as the functional constituent for the fabrication of fully green BC-CH nanocomposites with antibacterial properties (Adamczak et al., 2019; Lu et al., 2019).

Glycyrrhizic acid (GA), a natural triterpenoid saponin derived from the root of the licorice plant, is widely used as food additives (sweeteners) in candies and sweets, or as a drug for treating liver and skin diseases. GA has various biological activities, such as anti-inflammation, hepatoprotective, anticancer, antioxidant, and antiviral effects (Bailey and Vergoten, 2020; Li et al., 2023; Baltina et al., 2009). Chemically, GA molecules possess a typical amphiphilic structure composed of a hydrophobic triterpenoid aglycon moiety (18 β -glycyrrhetic acid) and a hydrophilic diglucuronic acid, which endows them with an interesting hierarchical self-assembly behavior in water (Li et al., 2021; Li et al., 2022). Previous studies have shown that amphiphilic GA can assemble into long semiflexible nanofibrils (2.5 nm thickness), which further form a supramolecular hydrogel at a concentration over 0.3 wt% (Wan et al., 2017a; Xu et al., 2022; Su et al., 2021). Berberine (BR), also known as berbamine, is a quaternary ammonium alkaloid extracted from Chinese medicinal herbs such as *Coptis chinensis*, *Phellodendron amurense*, and *Berberis vulgaris*. As a natural antibacterial agent, BR exhibits anti-inflammatory and broad-spectrum antimicrobial properties, as well as favorable biocompatibility and biodegradability (Kumar et al., 2015). Tannic acid (TA) is a natural polyphenol extracted from various plants, and has diverse biological activities, such as antioxidant, antibacterial, antiviral, and hemostatic properties. Its abundant phenolic hydroxyl can facilitate the formation of noncovalent interactions (e.g., ionic pairing,

hydrophobic and hydrogen-bonding interactions) with a wide range of molecules including alkaloids, saponins, polysaccharides, and proteins (Yan et al., 2020). Previous studies have indicated that these natural plant-based bioactive small molecules possess high reactivity with the tendency to form noncovalent interactions among each other, which can lead to the formation of insoluble precipitates or stable colloidal particles (Patel et al., 2012a,b; Hou et al., 2022). Patel et al. reported that GA, BR, and TA can form stable ternary colloidal nanoparticles via the spontaneous molecular interactions, and the co-assembled GA-BR-TA nanoparticles (GBTPs) can be facilely fabricated by simply mixing the aqueous solutions of these three natural bioactives (Patel et al., 2012b). The colloidal nanoparticles made of natural bioactive molecules are expected to have the ability as functional nanoscale building blocks, e.g., antibacterial nanoparticles, for the development of advanced nanocomposites.

Therefore, in this study, we incorporated the all-natural bioactive nanoparticle, GBTPs, into the dual nanofibril system of BC and CH nanofibrils, with the aim of fabricating the functional BC-CH nanocomposites with antibacterial activity. The GBTPs were first prepared from the co-assembly of three natural active small molecules, i.e., GA, BR, and TA. The BC-CH-GBTPs composite membranes were then fabricated by a facile, scalable, and ecofriendly papermaking process, which contains a simple vacuum filtration of the composite nanofibril-nanoparticle suspensions, followed by rapid drying on a semi-automatic sheet former. The mechanical and structural properties of the prepared BC-CH-GBTPs nanocomposites were characterized, and their antibacterial properties were finally evaluated. The BC-CH-GBTPs nanocomposites based on all-natural, plant-based building blocks are expected to find potential applications as active packaging materials with high safety.

2. Materials and methods

2.1. Materials

Bacterial cellulose (BC) was provided by Hainan Guangyu Biotechnology Co., Ltd., China. Chitin (CH) was provided by Shandong Aokang Biotechnology Co., Ltd., China. Glycyrrhizic acid (GA), berberine (BR), and tannic acid (TA) were purchased from Sigma Chemical Co. (St. Louis, MO, USA). All other chemicals used were of analytical grade.

2.2. Preparation of bacterial cellulose (BC) nanofibrils

The residual culture medium, bacteria, and impurities on BC pellicles were washed off with purified water (Milli-Q, Millipore Corp., Bedford, MA, USA) and then soaked in 0.2 M NaOH (Sinopharm Chemical Reagent Co., Ltd, Shanghai, China) solution at 90 °C for 30 min. Then, the purified BC was mixed with purified water at a 1:1 mass ratio, and the mixture was subjected to high-speed shearing at 12000 rpm for 10 min using a high-speed homogenizer (Ultra-Turrax T25, IKA-Werke GmbH & Co., Germany). Then, the sample was further treated using a colloid mill (IKA LABOR-PILOT, 2000/4, Germany) for 30 min to facilitate the defibrillation. Finally, the homogeneous suspension of BC nanofibrils was obtained by further homogenizing the sample at 20000 psi for 10 passes using an M-110EH-30 microfluidizer processor (Microfluidics, Newton, MA, USA). The prepared BC suspension was stored at 4 °C in a refrigerator before use.

2.3. Preparation of chitin (CH) nanofibrils

The CH nanofibrils were prepared according to the method described in our previous work (Yuan et al., 2014). Briefly, 1.0 g of CH powder was dispersed in 99.0 g of water, and the pH was adjusted to 3.0 using acetic acid (Macklin Biochemical Technology Co., Ltd, Shanghai, China). A pH meter (S20-SevenEasy, Mettler Toledo, Switzerland) was used for accurate pH control. After stirring for 10 min at 300 rpm with a magnetic

stirrer (RCT basic, IKA, Germany), the slurry was subjected to shearing at 10000 rpm for 5 min using the Ultra-Turrax T25 homogenizer. The resulting mixture was further processed by microfluidization (M-110EH-30 Microfluidics) at 20000 psi for 10 passes, and then the suspension of CH nanofibers was obtained and stored at 4 °C in a refrigerator before further use.

2.4. Preparation of glycyrrhizic acid-based bioactive nanoparticles (GBTPs)

GBTPs were prepared according to the experimental procedure described by Patel et al. (2012b). GA, BR, and TA powders were completely dissolved in purified water by stirring at room temperature (25 °C) for 30 min, respectively, to obtain the resulting stock solutions (10 mM). GA solution was first slowly added to TA solution, followed by a full reaction for 2 h. Then, BR solution was slowly added to the resultant GA-TA mixture. These solutions were mixed at a volume ratio of 1:1:1 under a magnetic stirring for 10 min at 1000 rpm. The pH value of the mixed solutions was maintained at 3.5 by using 0.1 M HCl solution during the fabrication process. GBTPs suspension was finally obtained at a concentration of 10 mM and were kept at 4 °C in a refrigerator for further use or freeze-dried into powder for structural characterization.

2.5. Preparation of BC-CH-GBTPs composite membranes

To prepare the BC-CH-GBTPs nanocomposites, the BC and CH nanofibrils suspensions were first mixed at a mass ratio of 1:1 to obtain the mixture with a nanofibril concentration of 0.1 wt% and a total mass of 60 g. Next, an appropriate amount of GBTPs suspension was added to the BC-CH nanofibril mixture to obtain the homogeneous BC-CH-GBTPs suspensions. The mixture was magnetically stirred for 1 h at 600 rpm and then sonicated (JY98-IIID, Xinzhi Biotechnology Co., Ltd, China) at 100 W for 10 min to ensure a homogeneous suspension. The resulting BC-CH-GBTPs suspension was then filtered through a Durapore® membrane filter (0.65 µm, PVDF, Millipore, USA) to form wet hydrogel films. The hydrogel films were subsequently dried in a semi-automatic sheet former (Rapid-Köthen, Austria) for 10 min (90 °C, 0.1 MPa). After drying, the obtained composites were placed in a desiccator (50% relative humidity, 25 °C) for 48 h before further characterization. The composite membranes were labeled as 10% GBTPs, 30% GBTPs, and 50% GBTPs, respectively, based on the concentration of GBTPs used in nanocomposites (10, 30, and 50 wt % BC-CH, respectively). A pure BC-CH membrane was used as the control group.

2.6. Particle characterization of GBTPs

GBTPs suspension was diluted to 2 mM, and then 5 µL of the sample was added dropwise to the copper grid. The excess liquid was aspirated with filter paper (Situofan Biotechnology Co., Ltd., Hangzhou, China) after 30 s. Subsequently, 5 µL of the 1% uranyl acetate (Guangdong Fangxin Biotechnology Co., Ltd., Shantou, China) was placed on the grid and removed after 30 s. The sample was observed at 100 kV on a JEM-2100F transmission electron microscope (TEM, JEOL, Japan). A UV spectrophotometer (Genesys 10S, Thermo, USA) was used to measure the UV spectra of GA, BR, TA, and GBTPs solutions, with the scanning wavelength range of 200–600 nm.

2.7. Characterization of BC-CH-GBTPs nanocomposites

2.7.1. Mechanical properties

The mechanical properties of the composite membranes were analyzed on a universal tensile testing machine (Instron 5565, USA) using a 100 N load cell according to ASTM D882 (2012). All membranes were cut into rectangular strips of 40 mm × 5 mm, with the initial distance set to 10 mm and the stretching speed set to 0.5 mm/s. The thickness of the membranes was measured using a Lorentzen & Wettre

Micrometer 250 (Sweden). Based on the force-distance data, Young's modulus (YM), tensile strength (TS), and elongation at break (EAB) were determined from the stress-strain curves using the following equations:

$$YM = \frac{\text{Stress}}{\text{Strain}} = \frac{F/A}{\Delta L - L} \quad (1)$$

$$TS = \frac{F_{\max}}{A} \quad (2)$$

$$EAB = \frac{\Delta L}{L} \quad (3)$$

where F, A, ΔL, L, F_{max} are the force applied to the structure, the cross-sectional area of the film, the change in length of the film when the force is applied, the initial length, and the maximum tensile force. Eight specimens of each membrane were tested and the calculated average value was used as the mechanical parameters of the samples.

2.7.2. Field-emission scanning electronic microscopy (FE-SEM)

Field-emission scanning electron microscopy (JEOL JFC-1200 fine coater, Japan) was employed to observe the microstructure of the membrane surface. The composites were sputtered with gold for 10 min and then placed in the SEM chamber at a voltage of 15 kV, and a magnification of 10000 × was used for observation.

2.7.3. Atomic force microscopy (AFM)

The morphology and roughness of the membrane surface were characterized using a MultiMode 8 scanning probe microscope (Bruker, USA). The composite film was cut into 5 mm × 5 mm pieces and fixed onto the carrier table. A 3 µm × 3 µm area was scanned at 25 °C and imaged using tapping mode. The acquired images were analyzed using Nanoscope Analysis software to obtain surface microstructure and roughness information.

2.7.4. Water contact angle (WCA)

WCA values on the membrane surface were measured by using a DataPhysics Instrument (OCA 20, Germany). A drop of water (5 µL) was put on the membrane surface and the drop images were recorded with a high-speed camera for analysis with Laplace-Young equation. Each sample was tested at least six times, and the average value was calculated.

2.7.5. Fourier transform infrared (FTIR) spectroscopy

FTIR spectra of GA, BR, TA, GBTPs, and composites were measured using the total reflection component of the VERTEX 70 FTIR spectrometer (Bruker, Germany), with the scanning range of 400–4000 cm⁻¹.

2.7.6. Thermogravimetric (TG) analysis

Thermal properties of the samples were determined using a simultaneous thermal analyzer (TG209F1, Germany). Samples for measurements were weighed about 5 mg per sample and placed in Al₂O₃ crucibles. The heating ramp-up rate and temperature range were set to 20 °C/min and 30–600 °C, respectively. Nitrogen was used as the atmosphere.

2.7.7. Antibacterial test

The antimicrobial properties of bioactive nanocomposites were determined according to the method described in our previous work (Li et al., 2020). Antimicrobial activity was evaluated by using the inhibition zone. Small discs of different composite membranes (6 mm diameter) were first sterilized under UV radiation for 30 min on both sides. 100 µL of *Escherichia coli* and *Staphylococcus aureus* suspensions diluted with phosphate buffered saline (PBS) buffer (pH 7.8) at a concentration of 10⁵ CFU/mL were then pipetted onto a Petri dish, respectively, and the suspension was mixed with Luria-Bertani (LB) solid medium cooled

to 40–50 °C. After the medium was solidified, small discs of the sterilized composites were placed on the surface of the medium. The Petri dishes containing the composite membranes were incubated in an orbital shaker (IKA KS 4000 IC Control, Staufen, Germany) at 37 °C for 24 h and after that, the inhibition zones around the membranes were recorded, photographed and their diameter values were exactly measured. All tests were performed in triplicate for each sample.

2.8. Statistical analysis

All measurements were carried out in triplicate. The data were assessed by an analysis of variance (ANOVA) by using SPSS 19.0 statistical analysis system. Duncan's multiple range test was adopted for comparison of mean values among three treatments using a level of significance of 5%.

3. Results and discussion

3.1. Formation of GA-BR-TA nanoparticles (GBTPs)

Natural bioactive substances can spontaneously interact with each other due to their structural features, which often leads to the formation of insoluble precipitates (Hou et al., 2022). It has been demonstrated that the aggregation and precipitation of TA and BR are mediated by strong non-covalent interactions including hydrogen bonding and π - π stacking interactions (Chen et al., 2022). For amphiphilic GA molecules, they have a hierarchical self-assembly behavior in water and can form long semiflexible nanofibrils in water (Fig. 1a). Previous study showed that the presence of amphiphilic GA molecules can provide steric stabilization for the TA-BR complex by adsorbing on the particle surface and interacting with both TA and BR, thereby forming stable colloidal nanoparticles (Patel et al., 2012b). As expected, it can be observed from Fig. 1b (inset image) that the nanoparticles (GBTPs) were formed from the GA-BR-TA ternary system, which are mostly spherical with a

diameter of 50–100 nm as well as a relatively uniform size distribution. The obtained GBTPs suspension is stable with a homogeneous appearance and shows a bright yellow color, mainly due to the color of BR solution.

Fig. 1c displays the characteristic absorption peaks of GA, BR, and TA at 257, 228/262, and 212/275/343 nm, respectively. The UV spectrum of GBTPs exhibited all the characteristic peaks of GA, BR, and TA, indicating the simultaneous presence of these three components in GBTPs. Notably, the absorption peak of GBTPs was red-shifted to 271 nm compared to the those of GA (257 nm) and BR (262 nm), suggesting the occurrence of non-covalent interactions among the system. Further investigation of the intermolecular interactions involved in the formation of GBTP was carried out using FTIR. As shown in Fig. 1d, GA and BR displayed characteristic peaks at 3442, 1718, 1622, 1358, and 1018 cm^{-1} , which correspond to the vibrations of O–H stretching, C=O stretching, C=C stretching, C–O stretching, and C–O–C stretching, respectively. In addition to these typical absorption peaks, TA exhibited a distinctive peak at 2922 cm^{-1} , due to the O–H stretching vibration and C–H antisymmetric stretching of COOH groups (Yang et al., 2021). The spectra of GBTPs showed distinctive peaks at 1080 cm^{-1} (C–O–C) and 1622 cm^{-1} (C=C). The characteristic peak (C=O) of GBTPs at 1718 cm^{-1} disappeared, suggesting that the C=O bond was involved in the molecular interactions during the non-covalent assembly of GA, BR, and TA to form GBTPs. The characteristic peak around 3400 cm^{-1} indicates the formation of hydrogen bonds, and the hydroxyl vibration peak of GBTPs was shifted to a lower wavenumber (3432 cm^{-1}) as compared to those of GA, BR, and TA (3442 cm^{-1} and 3445 cm^{-1}), which implies the occurrence of intermolecular hydrogen bonds in GBTPs.

3.2. Fabrication and mechanical properties of BC-CH-GBTPs nanocomposites

Fig. 2 shows the schematic diagram of a simple and facile paper-making process for fabricating BC-CH-GBTPs nanocomposites. In brief,

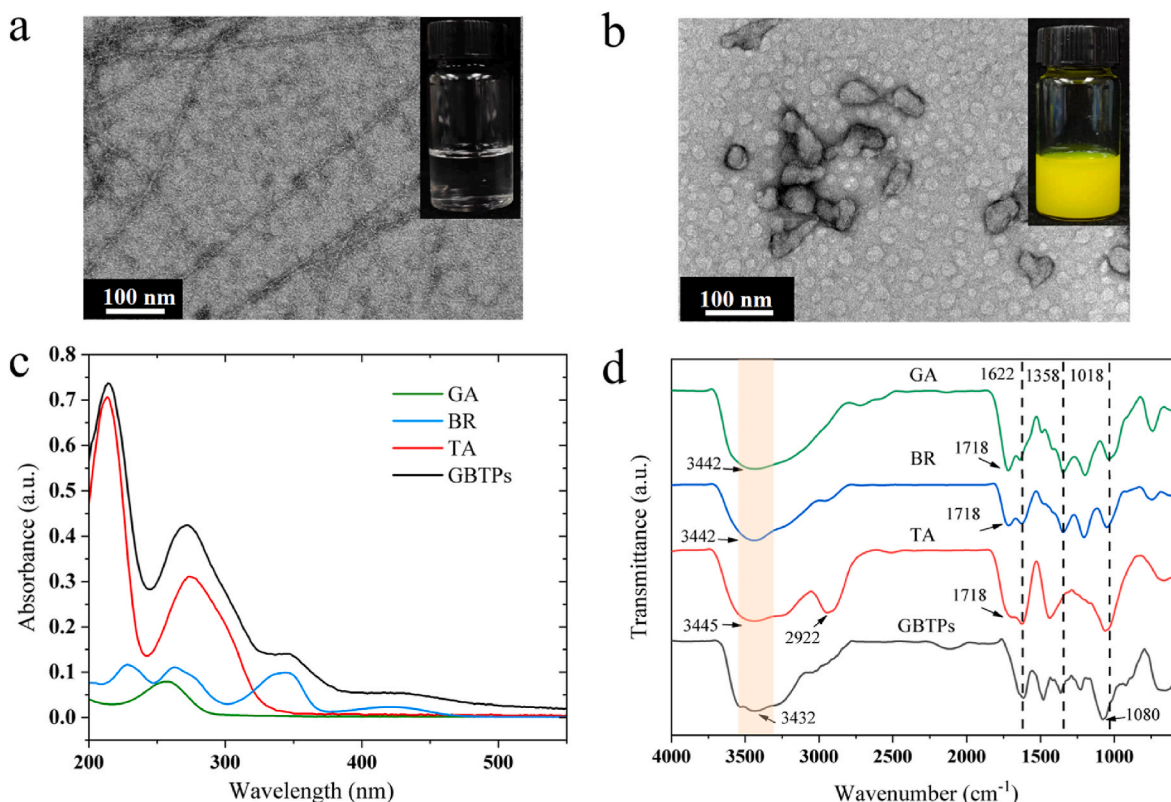


Fig. 1. TEM images and inset photographs of GA (a, 10 mM) and GBTPs (b, 10 mM) nanofibrils suspensions. (c) UV and (d) FTIR spectra of GA, BR, TA and GBTPs.



Fig. 2. Schematic illustration of preparation process of BC-CH-GBTPs nanocomposites. (1) Formation of GBTPs; (2 and 3) high-pressure microfluidization for preparing BC and CH nanofibrils, respectively; (4) mixing the as-synthesized suspensions of BC and CH; (5) mixing the GBTPs and suspensions of BC-CH; (6) hot-pressing at 90 °C and 0.1 MPa on a semiautomatic paper machine (Rapid-Köthen). AFM images and inset photographs of BC (a, 0.2 wt%) and CH nanofibrils (b, 0.2 wt%).

aqueous solutions of TA, GA, and BR were mixed in a volume ratio of 1:1:1 in sequence to prepare nanoparticles GBTPs. To obtain a homogeneous dual nanofibril system, a high-pressure microfluidic processor

was utilized to mechanically defibrillate the interconnected nanofiber network, resulting in the formation of uniform BC and CH nanofibril suspensions (Wu et al., 2014). GBTPs were then combined with the

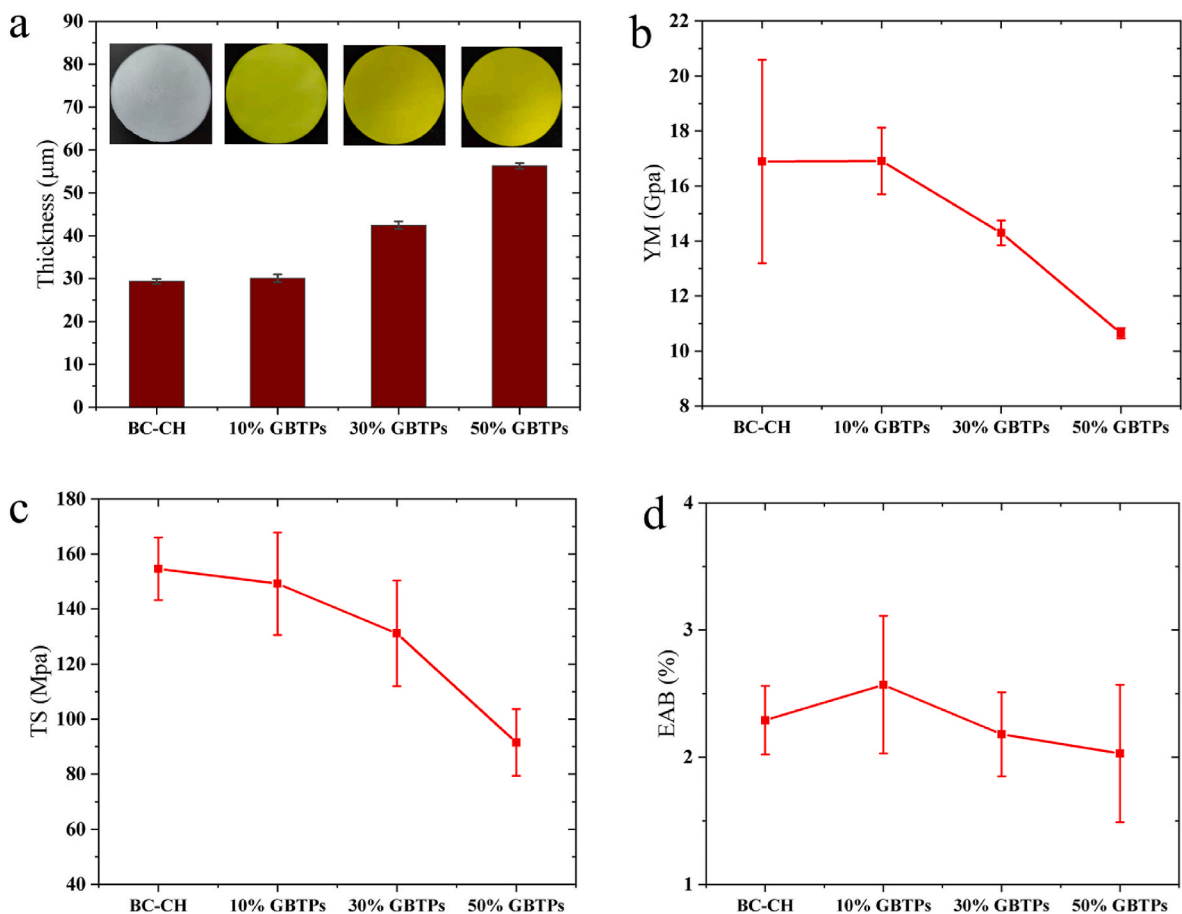


Fig. 3. (a) Thickness and (b–d) mechanical parameters of BC-CH and BC-CH-GBTPs nanocomposites with different GBTPs contents (10–50 wt% BC-CH). Inset images in (a) show the appearances of BC-CH-GBTPs nanocomposites.

BC-CH nanofibril suspensions to create a stable and homogeneous BC-CH-GBTPs composite system. Finally, the BC-CH-GBTPs composite suspension was vacuum filtered and then dried on a paper-making machine, and after that, the BC-CH-GBTPs nanocomposite membranes were effectively produced (Fig. 3a, see inset images). In comparison with the conventional preparation methods of immersing BC into a CH solution or co-cultivating BC with the presence of CH in culture medium (Yang et al., 2020; Yin et al., 2020), the present employed paper-making process for synthesizing BC-CH-GBTPs nanocomposites offers the advantages of simplicity, precise control over the ratio of BC, CH, and GBTPs, and environmental sustainability. It also holds the potential for large-scale production of stable nanocomposites, overcoming limitations of low production efficiency and complex preparation procedures (Li et al., 2020). The incorporated GBTPs particles are derived entirely from all-natural active small molecules that have various biological effects (e.g., antibacterial effect), which are expected to endow the final nanocomposites with antibacterial activity.

As seen from the inset images of Fig. 3a, the prepared BC-CH-GBTPs nanocomposites showed intact appearances with a smooth surface as well as a uniform yellow color, indicating that the GBTPs were mostly incorporated into the BC-CH fibrillar network during the vacuum filtration. Compared to pure BC-CH membrane ($29.34 \pm 0.59 \mu\text{m}$), the thickness of the nanocomposite with 10% GBTPs ($30.07 \pm 0.91 \mu\text{m}$) remained relatively constant. This may be attributed to the presence of network voids of BC-CH system, which could be filled by the addition of a small amount of GBTPs and thus results in no significant increase in membrane thickness. Upon further increase in the GBTPs amount (30 and 50%), the thickness of composite membranes ($42.45 \pm 0.89 \mu\text{m}$ and $56.29 \pm 0.66 \mu\text{m}$, respectively) increased significantly ($p < 0.05$) as expected. The mechanical properties of film materials are critical for their practical applications (Li et al., 2020), and the suitability and reliability of films in different application environments can be evaluated based on their mechanical parameters including Young's modulus

(YM), tensile strength (TS), and elongation at break (EAB). As can be seen in Fig. 3b–d, the addition of 10% GBTPs does not affect the mechanical properties of the nanocomposites significantly. When the amount of GBTPs exceeds 30%, the attenuation of these parameters of nanocomposites becomes statistically significant ($p < 0.5$). The presence of 50% GBTPs leads to an obvious decrease in the TS value of the nanocomposite ($91.55 \pm 12.12 \text{ MPa}$, Fig. 3c) as compared to that of BC-CH membrane ($154.60 \pm 11.43 \text{ MPa}$), and the corresponding YM and EAB values of the membranes decreased from 16.89 ± 3.70 to $10.65 \pm 0.19 \text{ GPa}$ (Fig. 3b) and from $2.29 \pm 0.27\%$ to $2.03 \pm 0.54\%$ (Fig. 3d), respectively. Similar phenomena were also observed in the composite material of BC/chitosan and curcumin nanoparticles (Yang et al., 2020). The addition of GBTPs results in an increased volume of the BC-CH membrane, which reduces its density and may decrease the binding degree and weaken the hydrogen bonding between the nanofibrils, thereby impairing the mechanical properties of nanocomposites to some extent. However, it should be noted that the overall mechanical performance of the BC-CH-GBTPs nanocomposites is still satisfactory.

3.3. Structural properties of BC-CH-GBTPs nanocomposites

Fig. 4 displays the FE-SEM images of the surfaces of the BC-CH-GBTPs nanocomposites. The microfluidization process breaks down original BC and CH into individual nanofibrils (Fig. 2), which contribute to the formation of a fibrous network structure. In addition, the positively charged CH nanofibrils can readily adsorb onto the negatively charged BC nanofibrils through electrostatic interactions. During vacuum filtration and drying, the fibrils are randomly arranged, overlapping, and woven into a dense three-dimensional network membrane structure (Fig. 4a). With the addition of 10% GBTPs, it can be seen that the small GBTPs nanoparticles appear to be evenly distributed in the fibrous network (Fig. 4b), which is overall similar to the original BC-CH membrane network (Fig. 4a). Upon further increase of GBTPs contents

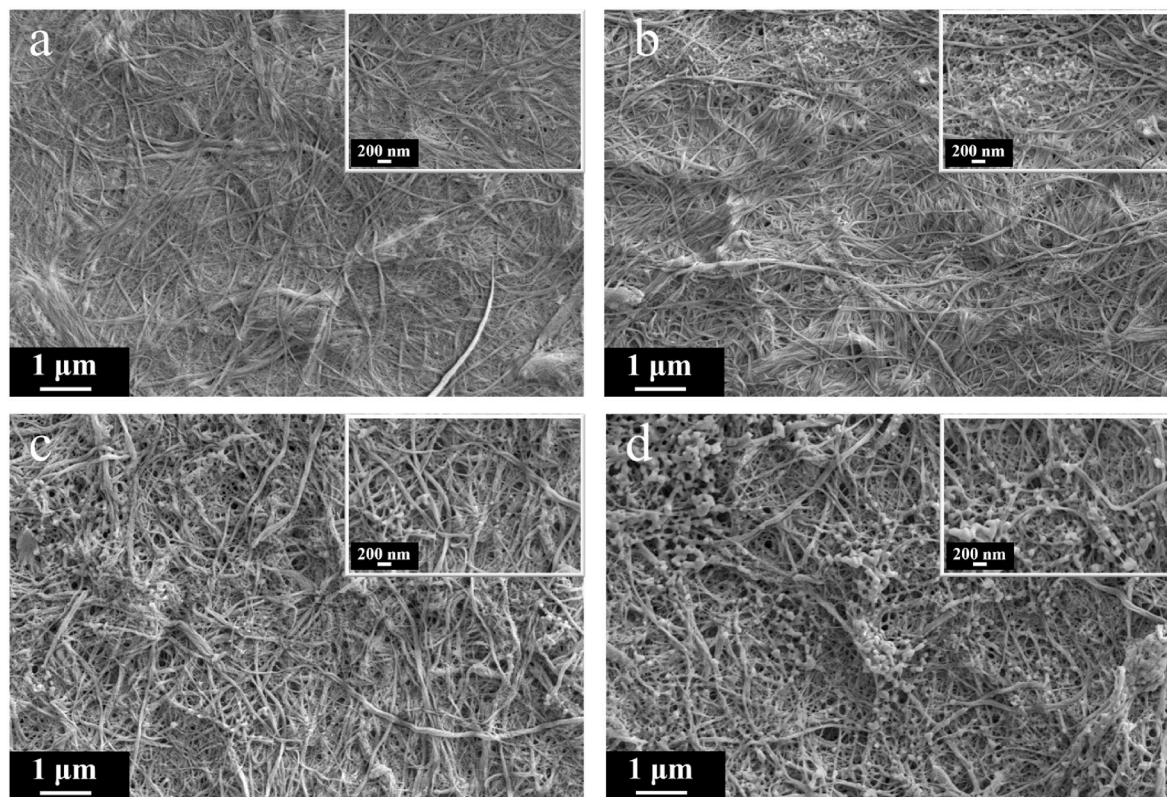


Fig. 4. FE-SEM images (scale bar = 1 μm) of (a) BC-CH, (b) BC-CH-10% GBTPs, (c) BC-CH-30% GBTPs, and (d) BC-CH-50% GBTPs nanocomposite surfaces. Insets in (a–d) show the high-resolution SEM images (scale bar = 200 nm) of nanocomposite surfaces.

(30 and 50%), the integrated and large GBTPs nanoparticles and particle aggregates can be clearly observed from the surfaces of nanocomposites (Fig. 4c and d), leading to an uneven surface with significantly different morphologies. It is worth noting that the presence of high amounts of GBTPs (30 and 50%) increased the pore size of the nanocomposites, leading to a looser network structure with reduced compactness, as compared to that of the BC-CH nanocomposite. This change in microstructure is indicative of the decrease in the mechanical properties of nanocomposites caused by high GBTPs contents (30–50%), as shown in Fig. 3.

AFM observation of the membrane surfaces can provide not only a more intuitive microstructure information but also a quantified analysis of the surface roughness of the membrane. Fig. 5 shows the two-dimensional AFM images of BC-CH and BC-CH-GBTPs nanocomposite membranes. The height of the membrane surface within the scanning range is represented by the brightness of the image, and the brighter image means the higher actual height. Compared with the relatively smooth and flat BC-CH membrane (Fig. 5a), the addition of GBTPs leads to a higher surface roughness of the nanocomposites (Fig. 5b–d), which may facilitate improving their surface hydrophobicity. According to the calculated parameters of surface roughness shown in Fig. 5e, the values of root-mean-square roughness (R_q) and average roughness (R_a) both increased after the addition of GBTPs, showing an increasing trend with increasing GBTPs concentration. This is well consistent with the FE-SEM (Fig. 4) and AFM (Fig. 5a–d) observations. Further evaluation of the effect of GBTPs on the surface wettability of the nanocomposites was performed by measuring the values of water contact angle (WCA). The WCA value of pure BC membrane was only 28.70° (Li et al., 2020), suggesting a highly hydrophilic surface. The WCA of the BC-CH composite increased to 48.13° , which is mainly due to the interaction between CH and BC nanofibrils and thus reduces the free hydrophilic groups of BC (Azarifar et al., 2019). As shown in Fig. 5b, the addition of GBTPs can further enhance the hydrophobicity of the BC-CH membrane, and the WCA ($48.13\text{--}59.80^\circ$) increased with increasing GBTPs contents. This is mainly because the surfaces of the nanocomposites become rougher after the addition of GBTPs (especially at 50%), and the space between particle aggregates can trap the air to further increase the

surface hydrophobicity of nanocomposites (Fu et al., 2015; Wan et al., 2017b).

FTIR was then used to analyze the surface chemical structure of the nanocomposites. As shown in Fig. 6a, for the BC-CH membrane, the obvious characteristic peaks at 1027 cm^{-1} , 2895 cm^{-1} , and 3327 cm^{-1} correspond to the C–H bending, C–O stretching, C–H stretching of CH_2/CH_3 groups, and the stretching vibration of O–H, respectively. The peak observed at 3327 cm^{-1} suggests the formation of intramolecular hydrogen bonds between BC and CH. After the addition of GBTPs, it can be clearly observed that the intensity of the band at 3327 cm^{-1} significantly decreased, indicating a reduced amount of free hydroxyl groups on the surface of the nanocomposites, which can be explained by their involvement in the formation of hydrogen bonds with GBTPs. In addition, the reduced peak intensity at 2895 cm^{-1} due to the stretching of aliphatic CH groups as well as the disappeared characteristic peaks of GBTPs at $1000\text{--}1700\text{ cm}^{-1}$ (Fig. 1d) also point to the occurrence of strong intermolecular hydrogen-bonding interactions among GBTPs and BC-CH composites.

TG analysis was further carried out to evaluate the thermal stability of the BC-CN-GBTPs nanocomposites. As shown in Fig. 6b, there is a slight weight loss below 100°C for all samples, which is attributed to the drying of moisture from the membranes. For BC-CH membrane, two typical decomposition stages can be clearly observed. The first rapid decomposition occurred in the temperature range of around $240\text{--}395^\circ\text{C}$ due to the fiber depolymerization, glycosyl carbonization, and other events within the membrane (Abraal et al., 2018), and when the temperature exceeds 400°C , the further full decomposition of fibrils leads to the formation of various pyrolysis products. For the BC-CH-GBTPs nanocomposites, one can observe an additional weight loss phenomenon occurring at around 205°C , which is due to the decomposition of GBTPs. As the temperature increased, the weight loss curves of the nanocomposites were generally consistent with that of the BC-CH membrane. However, it is noted that compared to the BC-CH membrane with 78.1% weight loss, the residues of the BC-CH-GBTPs nanocomposites with 30 and 50% GBTPs increased, showing the weight loss values of 75.7% and 69.7%, respectively. In addition, these nanocomposites also showed lower weight loss rate, as seen from the

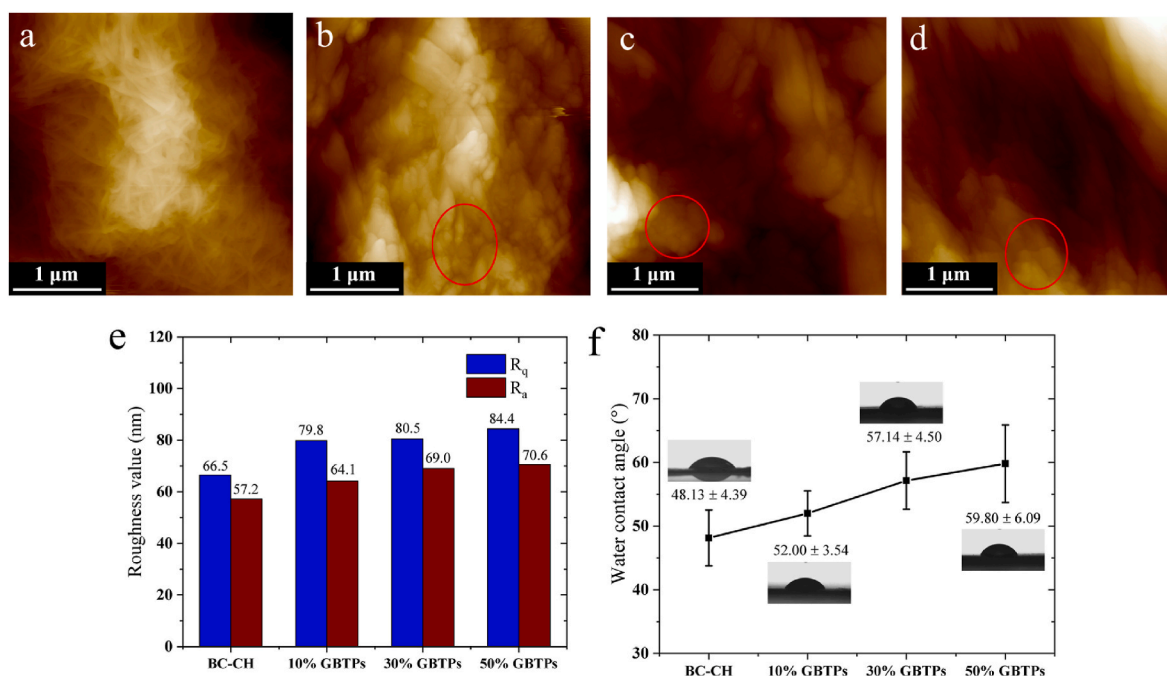


Fig. 5. 2D AFM images of the surfaces for (a) BC-CH, (b) BC-CH-10% GBTPs, (c) BC-CH-30% GBTPs, and (d) BC-CH-50% GBTPs nanocomposites. (e) R_q and R_a roughness values calculated from AFM images of BC-CH and the BC-CH-GBTPs nanocomposites with different GBTPs contents (10–50 wt% BC-CH); values calculated from at least three $5\ \mu\text{m} \times 5\ \mu\text{m}$ scans. (f) Water contact angles of these membranes.

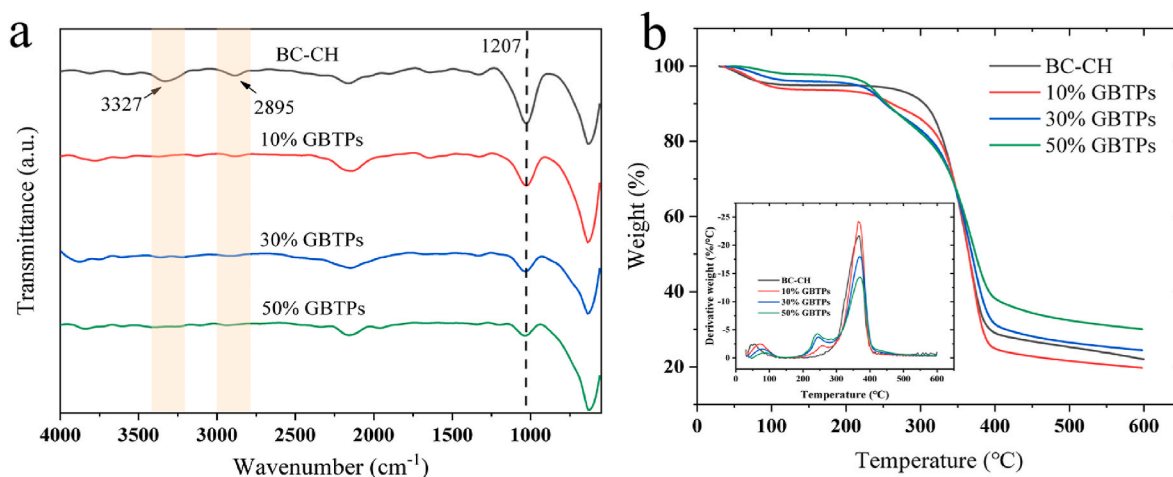


Fig. 6. (a) FTIR spectra and (b) TG analysis curves of BC-CH and the BC-CH-GBTPs nanocomposites with different GBTPs contents (10–50 wt% BC-CH).

derivative weight traces (inset in Fig. 6b). These results suggest that the incorporation of a higher content of GBTPs into the BC-CH fibrous network could promote the thermal stability of the final nanocomposites.

3.4. Antibacterial properties of BC-CH-GBTPs nanocomposites

Escherichia coli and *Staphylococcus aureus*, which are gram-positive and gram-negative bacteria, are often used to assess the broad-spectrum antibacterial characteristics of materials and are therefore selected as test bacteria. The inhibitory effects of the BC-CH-GBTPs nanocomposites on *Staphylococcus aureus* and *Escherichia coli* are

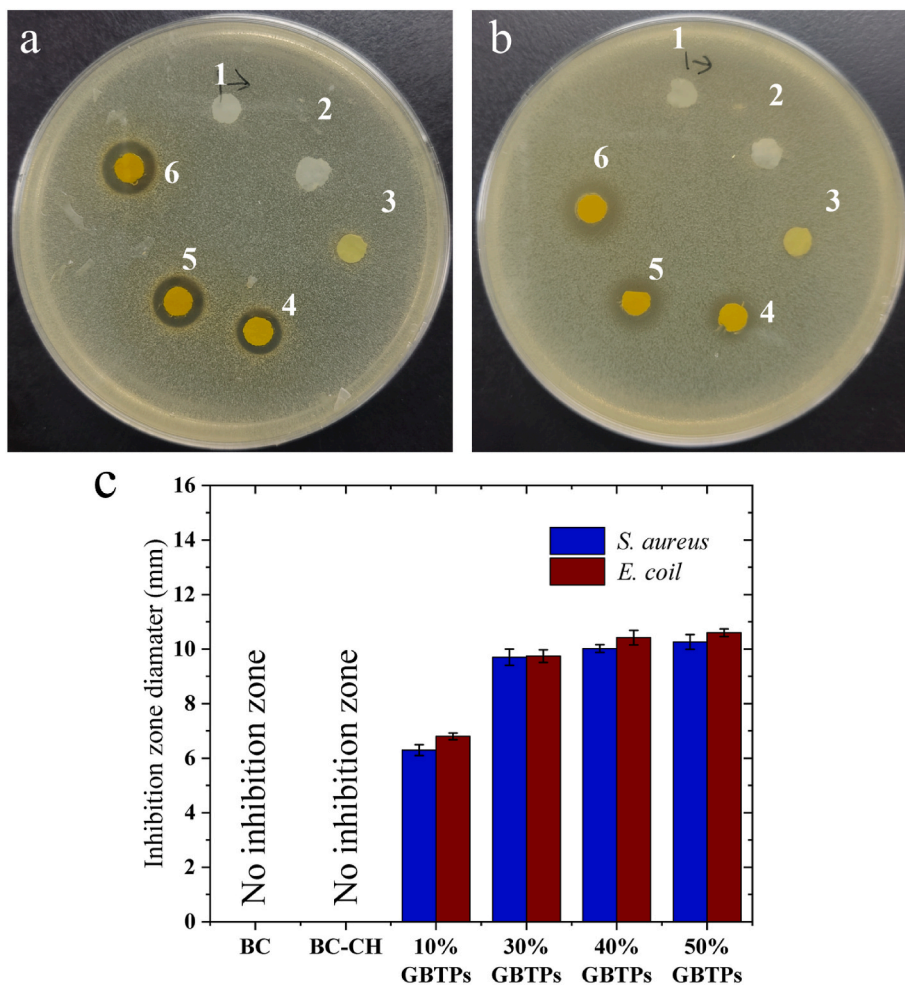


Fig. 7. Inhibition zones of BC-CH-GBTPs nanocomposites against *Staphylococcus aureus* (a) and *Escherichia coli* (b). Membrane: (1) BC, (2) BC-CH, (3) BC-CH-10% GBTPs, (4) BC-CH-30% GBTPs, (5) BC-CH-40% GBTPs, and (6) BC-CH-50% GBTPs. (c) Values of inhibition zone diameter of these samples.

depicted in Fig. 7a and b, respectively. As can be seen, pure BC did not exhibit antibacterial properties due to the lack of inherent antibacterial activity (Wang et al., 2018). Previous studies reported that CH has certain antibacterial ability (Yang et al., 2020), but the prepared BC-CH membrane did not show any inhibitory effect on the two types of bacteria. This is because the antibacterial ability of CH is closely related to the pH and the degree of deacetylation (DDA). Higher DDA values and lower pH values produce more cationic amino groups, thereby enhancing the antibacterial properties of chitosan nanofibrils (Xu et al., 2019). However, the CH nanofibrils used in this experiment were not partially deacetylated by sodium hydroxide treatment, and their incorporation into the network structure of nanocomposites also made them difficult to be released from the membrane (Yang et al., 2020), thus resulting in insufficient antibacterial activity. After the addition of GBTPs, the nanocomposites began to exhibit antibacterial properties, especially when the concentration of GBTPs was above 10%. As can be seen, the nanocomposites with higher concentrations of GBTPs (30–50% BC-CH) displayed an obvious antibacterial activity for both *Staphylococcus aureus* and *Escherichia coli*, and as expected, the diameters of the inhibition zones increased with increasing GBTPs concentration, showing an overall concentration-dependent inhibition behavior. This indicates that the incorporation of all-natural bioactive nanoparticles GBTPs can successfully endow the BC-CH nanocomposites with satisfactory antibacterial properties, which can have the potential as a green antibacterial material for applications in biomedicine or active food packaging (Zhao et al., 2019; Leite et al., 2021; Ma et al., 2022; Kirtil et al., 2021).

4. Conclusions

In summary, we have shown a facile and efficient fabrication of functional nanocomposite membranes by the incorporation of all-natural bioactive nanoparticles (GBTPs) into the dual nanofibril network of BC and CH nanofibrils. Bioactive GBTPs were obtained through the molecular self-assembly of three naturally occurring active small molecules, i.e., GA, BR, and TA, which can endow the final BC-CH-GBTPs nanocomposites with a significant inhibitory effect against *Escherichia coli* and *Staphylococcus aureus*, showing a satisfactory antibacterial ability. Additionally, the combination of GBTPs with the BC-CH fibrous matrix by hydrogen bonds did not compromise the structural integrity and to some extent can increase the thermal stability of the nanocomposites, which retained good mechanical and thermal properties. Furthermore, the addition of GBTPs led to a rougher surface structure and thus increased the water contact angle of the membrane surfaces, which can improve the surface hydrophobicity of BC-CH nanocomposites. These results suggest that the BC-CH-GBTPs nanocomposites based on all-natural, plant-based nanoscale building blocks, hold promising potentials as active membrane materials for sustainable applications in food and biomedical fields.

CRedit authorship contribution statement

Yuqi Mei: Methodology, Investigation, Data curation, Formal analysis, Writing – original draft. **Yunyi Yang:** Investigation, Data curation. **Ruohang Gao:** Methodology, Investigation, Data curation. **Mengyue Xu:** Formal analysis, Data curation. **Qing Li:** Formal analysis, Data curation. **Zhili Wan:** Validation, Writing – review & editing, Resources, Supervision, Funding acquisition, Project administration. **Xiaoquan Yang:** Resources, Project administration.

Declaration of competing interest

The authors declare no conflict of interest.

Data availability

Data will be made available on request.

Acknowledgments

This work was financially supported by the National Natural Science Foundation of China (32172347), the Natural Science Foundation of Guangdong Province (2021A1515011000), the Guangzhou Science and Technology Plan Project (202201010209), and the 111 Project (B17018).

References

- Abrial, H., Lawrensus, V., Handayani, D., Sugiarti, E., 2018. Preparation of nano-sized particles from bacterial cellulose using ultrasonication and their characterization. *Carbohydr. Polym.* 191, 161–167. <https://doi.org/10.1016/j.carbpol.2018.03.026>.
- Adamczak, A., Ozarowski, M., Karpiński, T.M., 2019. Antibacterial activity of some flavonoids and organic acids widely distributed in plants. *J. Clin. Med.* 9, 109. <https://doi.org/10.3390/jcm9010109>.
- Ahmad, S.I., Ahmad, R., Khan, M.S., Kant, R., Shahid, S., Gautam, L., Hasan, G.M., Hassan, M.I., 2020. Chitin and its derivatives: structural properties and biomedical applications. *Int. J. Biol. Macromol.* 164, 526–539. <https://doi.org/10.1016/j.ijbiomac.2020.07.098>.
- ASTM, 2012. ASTM D882-12, Standard Test Method for Tensile Properties of Thin Plastic Sheeting. <https://doi.org/10.1520/D0882-12.2>.
- Azarifar, M., Ghanbarzadeh, B., Khiabani, M.S., Basti, A.A., Abdulkhani, A., Noshirvani, N., Hosseini, M., 2019. The optimization of gelatin-CMC based active films containing chitin nanofiber and Trachyspermum ammi essential oil by response surface methodology. *Carbohydr. Polym.* 208, 457–468. <https://doi.org/10.1016/j.carbpol.2019.01.005>.
- Bai, L., Liu, L., Esquivel, M., Tardy, B.L., Huan, S., Niu, X., Liu, S., Yang, G., Fan, Y., Rojas, O.J., 2022. Nanochitin: chemistry, structure, assembly, and applications. *Chem. Rev.* 122, 11604–11674. <https://doi.org/10.1021/acs.chemrev.2c00125>.
- Bailey, C., Vergoten, G., 2020. Glycyrrhizin: an alternative drug for the treatment of COVID-19 infection and the associated respiratory syndrome? *Pharmacol. Ther.* 214, 107618. <https://doi.org/10.1016/j.pharmthera.2020.107618>.
- Baltina, L., Kondratenko, R., Plyasunova, O., Pokrovskii, A., Tolstikov, G., 2009. Prospects for the creation of new antiviral drugs based on glycyrrhizic acid and its derivatives (a review). *Pharm. Chem. J.* 43, 539–548. <https://doi.org/10.1007/s11094-010-0348-2>.
- Barhoum, A., Pal, K., Rahier, H., Uludag, H., Kim, I.S., Bechelany, M., 2019. Nanofibers as new-generation materials: from spinning and nano-spinning fabrication techniques to emerging applications. *Appl. Mater. Today* 17, 1–35. <https://doi.org/10.1016/j.apmt.2019.06.015>.
- Butchosa, N., Brown, C., Larsson, P.T., Berglund, L.A., Bulone, V., Zhou, Q., 2013. Nanocomposites of bacterial cellulose nanofibers and chitin nanocrystals: fabrication, characterization and bactericidal activity. *Green Chem.* 15, 3404–3413. <https://doi.org/10.1039/C3GC41700J>.
- Chen, L., Yu, H., Deutschman, C., Yang, T., Tam, K.C., 2020. Novel design of Fe-Cu alloy coated cellulose nanocrystals with strong antibacterial ability and efficient Pb²⁺ removal. *Carbohydr. Polym.* 234, 115889. <https://doi.org/10.1016/j.carbpol.2020.115889>.
- Chen, S., Chen, Z., Wang, Y., Hao, W., Yuan, Q., Zhou, H., Gao, C., Wang, Y., Wu, X., Wang, S., 2022. Targeted delivery of Chinese herb pair-based berberine/tannin acid self-assemblies for the treatment of ulcerative colitis. *J. Adv. Res.* 40, 263–276. <https://doi.org/10.1016/j.jare.2021.11.017>.
- Ding, F., Deng, H., Du, Y., Shi, X., Wang, Q., 2014. Emerging chitin and chitosan nanofibrous materials for biomedical applications. *Nanoscale* 6, 9477–9493. <https://doi.org/10.1039/C4NR02814G>.
- Fan, X., Guan, Y., Li, Y., Yu, H.Y., Marek, J., Wang, D., Militky, J., Zou, Z.Y., Yao, J., 2020. Shape-stabilized cellulose nanocrystal-based phase-change materials for energy storage. *ACS Appl. Nano Mater.* 3, 1741–1748. <https://doi.org/10.1021/acsnm.9b02441>.
- Fan, Y., Saito, T., Isogai, A., 2008. Chitin nanocrystals prepared by TEMPO-mediated oxidation of α-chitin. *Biomacromolecules* 9, 192–198. <https://doi.org/10.1021/bm700966g>.
- Fei, G., Wang, Y., Wang, H., Ma, Y., Guo, Q., Huang, W., Yang, D., Shao, Y., Ni, Y., 2019. Fabrication of bacterial cellulose/polyaniline nanocomposite paper with excellent conductivity, strength, and flexibility. *ACS Sustain. Chem. Eng.* 7, 8215–8225. <https://doi.org/10.1021/acssuschemeng.8b06306>.
- Fu, F., Li, L., Liu, L., Cai, J., Zhang, Y., Zhou, J., Zhang, L., 2015. Construction of cellulose based ZnO nanocomposite films with antibacterial properties through one-step coagulation. *ACS Appl. Mater. Interfaces* 7, 2597–2606. <https://doi.org/10.1021/am507639b>.
- Hou, Y., Zou, L., Li, Q., Chen, M., Ruan, H., Sun, Z., Xu, X., Yang, J., Ma, G., 2022. Supramolecular assemblies based on natural small molecules: union would be effective. *Mater. Today Bio* 15, 100327. <https://doi.org/10.1016/j.mtbio.2022.100327>.
- Ifuku, S., Saimoto, H., 2012. Chitin nanofibers: preparations, modifications, and applications. *Nanoscale* 4, 3308–3318. <https://doi.org/10.1039/C2NR30383C>.

- Kang, Y.J., Chun, S.J., Lee, S.S., Kim, B.Y., Kim, J.H., Chung, H., Lee, S.Y., Kim, W., 2012. All-solid-state flexible supercapacitors fabricated with bacterial nanocellulose papers, carbon nanotubes, and triblock-copolymer ion gels. *ACS Nano* 6, 6400–6406. <https://doi.org/10.1021/nn301971r>.
- Kirtil, E., Aydogdu, A., Svitova, T., Radke, C.J., 2021. Assessment of the performance of several novel approaches to improve physical properties of guar gum based biopolymer films. *Food Packag. Shelf Life* 29, 100687. <https://doi.org/10.1016/j.fpsl.2021.100687>.
- Klemm, D., Kramer, F., Moritz, S., Lindström, T., Ankerfors, M., Gray, D., Dorris, A., 2011. Nanocelluloses: a new family of nature-based materials. *Angew. Chem. Int. Ed.* 50, 5438–5466. <https://doi.org/10.1002/anie.201001273>.
- Kontturi, E., Laaksonen, P., Linder, M.B., Gröschel, A.H., Rojas, O.J., Ikkala, O., 2018. Advanced materials through assembly of nanocelluloses. *Adv. Mater.* 30, 1703779. <https://doi.org/10.1002/adma.201703779>.
- Kraemer, S.A., Ramachandran, A., Perron, G.G., 2019. Antibiotic pollution in the environment: from microbial ecology to public policy. *Microorganisms* 7, 180. <https://doi.org/10.3390/microorganisms7060180>.
- Kumar, A., Ekavali, Chopra, K., Mukherjee, M., Pottabathini, R., Dhull, D.K., 2015. Current knowledge and pharmacological profile of berberine: an update. *Eur. J. Pharmacol.* 761, 288–297. <https://doi.org/10.1016/j.ejphar.2015.05.068>.
- Leite, L.S.F., Pham, C., Bilatto, S., Azeredo, H.M., Cranston, E.D., Moreira, F.K., Mattoso, L.H.C., Bras, J., 2021. Effect of tannic acid and cellulose nanocrystals on antioxidant and antimicrobial properties of gelatin films. *ACS Sustain. Chem. Eng.* 9, 8539–8549. <https://doi.org/10.1021/acssuschemeng.1c01774>.
- Li, Q., Gao, R., Wang, L., Xu, M., Yuan, Y., Ma, L., Wan, Z., Yang, X., 2020. Nanocomposites of bacterial cellulose nanofibrils and zein nanoparticles for food packaging. *ACS Appl. Nano Mater.* 3, 2899–2910. <https://doi.org/10.1021/acsnm.0c00159>.
- Li, Q., Wan, Z., Yang, X., 2022. Glycyrrhizic acid: self-assembly and applications in multiphase food systems. *Curr. Opin. Food Sci.* 43, 107–113. <https://doi.org/10.1016/j.cofs.2021.11.008>.
- Li, Q., Xu, M., Xie, J., Su, E., Wan, Z., Sagis, L.M.C., Yang, X., 2021. Large amplitude oscillatory shear (Laos) for nonlinear rheological behavior of heterogeneous emulsion gels made from natural supramolecular gelators. *Food Res. Int.* 140, 110076. <https://doi.org/10.1016/j.foodres.2020.110076>.
- Li, Q., Zhang, S., Du, R., Yang, Y., Liu, Y., Wan, Z., Yang, X., 2023. Injectable self-healing adhesive natural glycyrrhizic acid bioactive hydrogel for bacteria-infected wound healing. *ACS Appl. Mater. Interfaces* 15, 17562–17576. <https://doi.org/10.1021/acsnami.2c23231>.
- Lu, L., Hu, W., Tian, Z., Yuan, D., Yi, G., Zhou, Y., Cheng, Q., Zhu, J., Li, M., 2019. Developing natural products as potential anti-biofilm agents. *Chin. Med.* 14, 1–17. <https://doi.org/10.1186/s13020-019-0232-2>.
- Lu, T., Gao, H., Liao, B., Wu, J., Zhang, W., Huang, J., Liu, M., Huang, J., Chang, Z., Jin, M., 2020. Characterization and optimization of production of bacterial cellulose from strain CGMCC 17276 based on whole-genome analysis. *Carbohydr. Polym.* 232, 115788. <https://doi.org/10.1016/j.carbpol.2019.115788>.
- Ma, K., Zhe, T., Li, F., Zhang, Y., Yu, M., Li, R., Wang, L., 2022. Sustainable films containing AIE-active berberine-based nanoparticles: a promising antibacterial food packaging. *Food Hydrocolloids* 123, 107147. <https://doi.org/10.1016/j.foodhyd.2021.107147>.
- Min, T.T., Zhou, L.P., Sun, X.L., Du, H.Y., Zhu, Z., Wen, Y.Q., 2022. Electrospun functional polymeric nanofibers for active food packaging: a review. *Food Chem.* 391, 15. <https://doi.org/10.1016/j.foodchem.2022.133239>.
- Patel, A.R., Drost, E., den Adel, R., Hazekamp, J., Velikov, K.P., 2012a. Temperature responsive colloidal particles from non-covalently interacting small molecular weight natural bioactive molecules. *Soft Matter* 8, 3515–3517. <https://doi.org/10.1039/C2SM25102G>.
- Patel, A.R., Seijen-ten-Hoorn, J., Heussen, P.C., Drost, E., Hazekamp, J., Velikov, K.P., 2012b. Straightforward preparation of organic colloidal particles by harnessing spontaneous non-covalent interactions of active molecules from natural origin. *J. Colloid Interface Sci.* 374, 150–156. <https://doi.org/10.1016/j.jcis.2012.01.056>.
- Shi, Z., Zhang, Y., Phillips, G.O., Yang, G., 2014. Utilization of bacterial cellulose in food. *Food Hydrocolloids* 35, 539–545. <https://doi.org/10.1016/j.foodhyd.2013.07.012>.
- Su, E., Li, Q., Xu, M., Yuan, Y., Wan, Z., Yang, X., Binks, B.P., 2021. Highly stable and thermo-responsive gel foams by synergistically combining glycyrrhizic acid nanofibrils and cellulose nanocrystals. *J. Colloid Interface Sci.* 587, 797–809. <https://doi.org/10.1016/j.jcis.2020.11.039>.
- Swingler, S., Gupta, A., Gibson, H., Kowalczyk, M., Heaselgrave, W., Radecka, I., 2021. Recent advances and applications of bacterial cellulose in biomedicine. *Polymers* 13, 29. <https://doi.org/10.3390/polym13030412>.
- Wahid, F., Huang, L.H., Zhao, X.Q., Li, W.C., Wang, Y.Y., Jia, S.R., Zhong, C., 2021. Bacterial cellulose and its potential for biomedical applications. *Biotechnol. Adv.* 53, 107856. <https://doi.org/10.1016/j.biotechadv.2021.107856>.
- Wan, Z., Sun, Y., Ma, L., Yang, X., Guo, J., Yin, S., 2017a. Responsive emulsion gels with tunable properties formed by self-assembled nanofibrils of natural saponin glycyrrhizic acid for oil structuring. *J. Agric. Food Chem.* 65, 2394–2405. <https://doi.org/10.1021/acs.jafc.6b05242>.
- Wan, Z., Wang, L., Ma, L., Sun, Y., Yang, X., 2017b. Controlled hydrophobic biosurface of bacterial cellulose nanofibers through self-assembly of natural zein protein. *ACS Biomater. Cell. Eng.* 3, 1595–1604. <https://doi.org/10.1021/acsbomaterials.7b00116>.
- Wan, Z., Wang, L., Yang, X., Guo, J., Yin, S., 2016. Enhanced water resistance properties of bacterial cellulose multilayer films by incorporating interlayers of electrospun zein fibers. *Food Hydrocolloids* 61, 269–276. <https://doi.org/10.1016/j.foodhyd.2016.05.024>.
- Wang, X., Xie, Y., Ge, H., Chen, L., Wang, J., Zhang, S., Guo, Y., Li, Z., Feng, X., 2018. Physical properties and antioxidant capacity of chitosan/epigallocatechin-3-gallate films reinforced with nano-bacterial cellulose. *Carbohydr. Polym.* 179, 207–220. <https://doi.org/10.1016/j.carbpol.2017.09.087>.
- Wu, J., Zhang, K., Girouard, N., Meredith, J.C., 2014. Facile route to produce chitin nanofibers as precursors for flexible and transparent gas barrier materials. *Biomacromolecules* 15, 4614–4620. <https://doi.org/10.1021/bm501416q>.
- Xu, J., Liu, L., Yu, J., Zou, Y., Wang, Z., Fan, Y., 2019. DDA (degree of deacetylation) and pH-dependent antibacterial properties of chitin nanofibers against *Escherichia coli*. *Cellulose* 26, 2279–2290. <https://doi.org/10.1007/s10570-019-02287-2>.
- Xu, M., Ma, L., Li, Q., Wu, J., Wan, Z., Ngai, T., Yang, X., 2022. Robust and highly adaptable high internal phase gel emulsions stabilized solely by a natural saponin hydrogelator glycyrrhizic acid. *Food Funct.* 13, 280–289. <https://doi.org/10.1039/d1fo01656c>.
- Yan, W., Shi, M., Dong, C., Liu, L., Gao, C., 2020. Applications of tannic acid in membrane technologies: a review. *Adv. Colloid Interface Sci.* 284, 102267. <https://doi.org/10.1016/j.cis.2020.102267>.
- Yang, F., Yang, J.C., Qiu, S., Xu, W., Wang, Y.T., 2021. Tannic acid enhanced the physical and oxidative stability of chitin particles stabilized oil in water emulsion. *Food Chem.* 346, 128762. <https://doi.org/10.1016/j.foodchem.2020.128762>.
- Yang, Y.N., Lu, K.Y., Wang, P., Ho, Y.C., Tsai, M.L., Mi, F.L., 2020. Development of bacterial cellulose/chitin multi-nanofibers based smart films containing natural active microspheres and nanoparticles formed in situ. *Carbohydr. Polym.* 228, 115370. <https://doi.org/10.1016/j.carbpol.2019.115370>.
- Yin, N., Du, R.P., Zhao, F.K., Han, Y., Zhou, Z.J., 2020. Characterization of antibacterial bacterial cellulose composite membranes modified with chitosan or chitooligosaccharide. *Carbohydr. Polym.* 229, 115520. <https://doi.org/10.1016/j.carbpol.2019.115520>.
- Yuan, Y., Sun, Y.E., Wan, Z.L., Yang, X.Q., Wu, J.F., Yin, S.W., Wang, J.M., Guo, J., 2014. Chitin microfibrils reinforce soy protein gels cross-linked by transglutaminase. *J. Agric. Food Chem.* 62, 4434–4442. <https://doi.org/10.1021/jf500922n>.
- Zhang, T., Wang, W., Zhang, D., Zhang, X., Ma, Y., Zhou, Y., Qi, L., 2010. Biotemplated synthesis of gold nanoparticle–bacteria cellulose nanofiber nanocomposites and their application in biosensing. *Adv. Funct. Mater.* 20, 1152–1160. <https://doi.org/10.1002/adfm.200902104>.
- Zhao, X., Zhang, H., Gao, Y., Lin, Y., Hu, J., 2019. A simple injectable moldable hydrogel assembled from natural glycyrrhizic acid with inherent antibacterial activity. *ACS Appl. Bio Mater.* 3, 648–653. <https://doi.org/10.1021/acsnm.9b01007>.